ELECTRIC POWER RESEARCH INSTITUTE

Plant Support Engineering: Flaw Tolerance Evaluation of Thermally Aged Cast Austenitic Stainless Steel Piping

1016236

Plant Support Engineering: Flaw Tolerance Evaluation of Thermally Aged Cast Austenitic Stainless Steel Piping

1016236

Technical Update, December 2007

EPRI Project Managers

P. O'Regan
N. Wilmshurst

ELECTRIC POWER RESEARCH INSTITUTE
3420 Hillview Avenue, Palo Alto, California 94304-1338 ▪ PO Box 10412, Palo Alto, California 94303-0813 ▪ USA
800.313.3774 ▪ 650.855.2121 ▪ askepri@epri.com ▪ www.epri.com

ORGANIZATION(S) THAT PREPARED THIS DOCUMENT

Structural Integrity Associates, Inc.

This is an EPRI Technical Update report. A Technical Update report is intended as an informal report of continuing research, a meeting, or a topical study. It is not a final EPRI technical report.

NOTE

For further information about EPRI, call the EPRI Customer Assistance Center at 800.313.3774 or e-mail askepri@epri.com.

CITATIONS

This document was prepared by

Structural Integrity Associates, Inc.
3315 Almaden Expressway, Suite 24
San Jose, CA 95118

Principal Investigators
N. G. Cofie
T. J. Griesbach

This document describes research sponsored by the Electric Power Research Institute (EPRI).

This publication is a corporate document that should be cited in the literature in the following manner:

Plant Support Engineering: Flaw Tolerance Evaluation of Thermally Aged Cast Austenitic Stainless Steel Piping. EPRI, Palo Alto, CA: 2007. 1016236.

PRODUCT DESCRIPTION

Cast austenitic stainless steel (CASS) materials are used in the primary system piping in about half of the PWRs in the United States. CASS piping systems are also used in PWRs in other countries such as Sweden, Japan, and France. CASS material is a good choice for the primary system piping based on its relative cost, toughness, and corrosion resistance. However, the microstructural and metallurgical characteristics that make CASS a good choice for toughness and corrosion resistance also hinder the ability to inspect the piping because of its coarse grain structure.

Recent improvements in phased array ultrasonic testing (UT) inspection are promising for their ability to detect flaws of reasonable size with a relatively high probability of detection and relatively low false call probability. Thus, it is important to determine appropriate target flaw sizes in the CASS piping and components in order to be able to demonstrate that there is no loss of structural integrity for long-term operation. The determination of these flaw sizes depends on the loading conditions and the toughness in the aged condition; CASS materials are known to be susceptible to thermal aging at the operating temperatures of PWRs (288–343°C). The toughness degradation is also a function of the chemical content (low or high molybdenum) and percent delta ferrite.

This report provides an update of the current state of knowledge on flaw tolerance evaluations of CASS piping systems. The update includes a review of prior work on this subject and the results of some recent studies. Considering typical loads that are normally associated with nuclear plant piping with CASS materials, it is concluded that, in general, the target flaw sizes in these components depend on the loads and safety margins used in the evaluation.

Results and Findings
The target flaw sizes for the cold leg piping considered in this study strongly depend on the loads and safety factor used in the analysis. For the case in which the safety margin is unity (that is, for critical flaw size), relatively large flaw sizes are obtained even with relatively high loads. When the ASME Code safety margin is applied, the target flaw sizes are smaller.

Challenges and Objectives
Because of their coarse grain structure, CASS piping has posed inspection challenges. Several attempts at inspecting these components using conventional inspection techniques have not been successful. Recent improvements in inspection technology using phased array UT techniques and eddy current techniques are promising for their ability to detect flaws of reasonable size with relatively high probability of detection and relatively low false call probability. Thus, it is important to determine appropriate target flaw sizes in the CASS piping and components to be able to demonstrate that there is no loss of structural integrity for long-term operation. With the improvements in inspection technology, the management of the long-term structural integrity of CASS components could be based on a combination of periodic inspections and flaw tolerance evaluations to determine the target flaw size that should be detected from the inspections.

Applications, Value, and Use
The management of the long-term structural integrity of CASS components will involve the combination of developing advanced inspection techniques and performing flaw tolerance

evaluations. The study described in this report provides a preliminary methodology for the flaw tolerance evaluation that—when used in concert with inspection techniques being developed by EPRI—can be used for the long-term management of CASS piping in the nuclear industry.

EPRI Perspective

This interim study has provided a preliminary methodology that can be used to determine target flaw sizes in CASS materials. Work envisioned for 2008 will use this study as a starting point. A key area to be addressed is determining whether a generic target flaw of reasonable size can be detected or if plant-specific analyses will be needed.

Approach

To perform the flaw tolerance evaluation, a typical cold leg piping for a PWR was considered in a fracture mechanics evaluation. The lower bound fracture toughness from a set of Grade CF8M CASS spool pieces was determined and used in the evaluation. The critical and allowable flaw sizes were calculated using elastic-plastic fracture mechanics techniques and limit-load analysis. Crack growth evaluation was also performed to determine the crack growth during the operating period.

Keywords

Cast austenitic stainless steel
Thermal embrittlement
Fracture toughness
Flaw tolerance
Critical flaw size
Allowable flaw size

CONTENTS

LIST OF FIGURES

LIST OF TABLES

1
INTRODUCTION

Cast austenitic stainless steel (CASS) components play a prominent role in light water reactor application as primary pressure boundary components. In boiling water reactors (BWRs), CASS components are used as pump casings and valve bodies, and in some instances, as elbows and as fittings. For pressurized water reactors (PWRs), the primary pressure boundary CASS applications include applications similar to those identified for BWRs, and can also involve cast piping components in some PWRs. CASS pumps, valves and fittings generally are fabricated from static castings due to the complex configurations involved, whereas in piping application, static and centrifugal castings can be used in these applications. CASS components are used widely in primary pressure boundary applications in light water reactor service as a result of reasonable cost combined with excellent resistance to corrosion effects and the excellent fracture toughness of CASS.

Among the excellent features of CASS are the corrosion resistance, including resistance to general corrosion, intergranular corrosion and stress corrosion cracking; improved resistance to sensitization when thermally treated; and the ease of welding of these materials. Since this material contains ferrite as one of the phases, the ferrite improves the corrosion resistance and improves the sensitization behavior of CASS and also facilitates weldability, and weld repair of these materials [1]. However, the ferrite phase also produces potentially detrimental effects on these materials as well. These effects include thermal embrittlement, toughness degradation and volumetric inspection issues.

Recent improvements in inspection technology using phased array UT [2] and eddy current techniques [3] are promising for the ability to detect flaws of reasonable size with relatively high probability of detection and relatively low false call probability. Thus, it is important to determine appropriate target acceptable flaw sizes in the CASS piping and components to be able to demonstrate no loss of structural integrity for long term operation. The determination of target flaw sizes depends on the loading conditions and the toughness in the aged condition; CASS materials are known to be susceptible to thermal aging at the operating temperatures of PWRs (288 – 343°C). The toughness degradation is also a function of the chemical content (low or high molybdenum) and percent delta ferrite. With the improvements in inspection technology, the management of the long term structural integrity of CASS components could be based on a combination of periodic inspections and flaw tolerance evaluation to determine the target flaw size that should be detected form the inspections.

This report provides an update of the current state of knowledge on flaw tolerance evaluations of CASS piping systems. The update includes a review of prior work on this subject and the results of some recent studies. Considering typical loads that are normally associated with nuclear plant piping with CASS materials, it is concluded that in general, the target flaw sizes in these components are dependent on the loads and safety margin used in the evaluation.

Section 2 provides background on the susceptibility of CASS to thermal aging and the factors that contribute to thermal embrittlement. Screening criteria to determine the most susceptible CASS material is also discussed. Section 3 provides the flaw tolerance evaluation approach and an example problem involving a cold leg piping is presented. Section 4 provides summary, conclusions and recommendations while Section 5 provides references used in the study.

2
THERMAL EMBRITTLEMENT SUSCEPTIBILITY OF CASS

Background on Thermal Embrittlement

Thermal embrittlement of the ferrite phase in CASS components occurs as a result of either a heat treatment at temperatures of less than 500 ºC (<932ºF) or as a result of long time aging at light water reactor primary coolant operating temperatures [4]. Various investigations have been performed examining the variables affecting the thermal embrittlement of CASS for various grades of cast components including CF-8, CF-8M, CF-3 and CF-3M stainless steels [4-7]. Studies investigating the cause of the embrittlement have demonstrated that thermal embrittlement of CASS can occur during the reactor design lifetime or life extension due to the formation of a Cr-rich ´ phase typically due to spinodal decomposition, nucleation and growth of ´; precipitation of a Ni- and Si-rich G phase, formation of $M_{23}C_6$ carbides and $_2$ (austenite), and/or additional precipitation and/or growth of existing carbides at the ferrite/austenite phase boundaries [4]. Within the family of CASS most often used in light water reactor application, low carbon CASS, CF-3 is the most resistant of these materials to thermal embrittlement and CF-8M, the molybdenum bearing higher carbon CASS material is the least resistant to thermal embrittlement [4]. One other important feature as related to thermal embrittlement of these materials is the quantity and distribution of the ferrite within the structure. When the ferrite phase is continuous, e.g., large ferrite content, or the ferrite/austenite phase boundary provides an easy path for cracking, the material is much more susceptible to brittle failure than when the material contains lower ferrite levels. In general, the decrease in toughness is generally not a significant concern in these alloys due to the extremely high toughness of the austenite matrix. Various studies have shown that higher ferrite contents correlate with increased susceptibility to embrittlement, and ferrite-forming elements such as Cr, Mo, Si, Cb and V increase the susceptibility to thermal embrittlement [4-7].

The formation of the ´ within the ferrite has its maximum effect at 475ºC (885ºF), and as such the phenomenon is identified as 475ºC embrittlement. Thermal aging causes the ductile to brittle transition temperature to increase and both room temperature and operating temperature toughness decrease with increasing embrittlement of the ferrite phase [1, 5]. Although the 475ºC temperature is significantly above the normal operating temperature of the BWR or PWR primary systems, a reduction in toughness of these materials due to the 475ºC embrittlement effects identified above can be observed following long time exposure to temperatures as low as 288ºC (550ºF).

Toughness Degradation

The reduction in toughness in CASS components in the as-fabricated condition is the result of the presence of a duplex grain structure (both austenite and ferrite) as well as the inherently lower toughness of the ferrite phase at operating temperatures. This effect is not generally a major concern, in the as-fabricated component, given the extremely high toughness of the austenite matrix [1]. A much greater concern is related to applications that result in exposure to higher temperatures, either as a result of a heat treatment, or as a result of prolonged operation at temperatures where thermal degradation can occur as discussed above.

The effect of thermal aging is to decrease the lower and upper shelf Charpy energy of CASS. The extent of the low temperature embrittlement is generally quantified by measuring the room temperature Charpy energy absorbed after aging at temperatures representative or slightly higher than those expected in service.

Since the ferrite phase is the only phase susceptible to thermal embrittlement, exposure to light water reactor operating temperatures for extended periods produces a structural effect due to thermal aging in the component which is dependent upon the quantity and morphology of the ferrite present. For light water rector applications, traditional guidelines have been that the low temperature embrittlement becomes a concern only when the volume fraction of the ferrite exceeds approximately 15 to 20%. The basis for this argument is that ferrite tends to form in pools in the austenite matrix and when ferrite levels are less than approximately 15%, there is significantly less likelihood that the embrittled ferrite phase can form a continuous path of embrittled material that can extend through the thickness of the cast component [5]. In addition, the size, distribution and morphology of the ferrite within the austenite matrix depend on the solidification conditions during the casting process. Cast stainless steels may solidify with a columnar or an equiaxed grain structure or a mixture of both structures. Investigators have observed that in CASS of similar chemical composition, the size and distribution of the ferrite islands within the austenite matrix tend to increase with larger section size. This effect is believed to be due to the slower heat removal rates observed in larger section thicknesses. With increased ferrite spacing at constant ferrite content, the size of the ferrite islands increases and the probability of a continuous path of ferrite through the thickness of the component increases [5].

Several investigators have focused on evaluating the effects of ferrite morphology, distribution and material composition on the toughness of CASS following long term exposures at reactor operating temperatures. Chopra [4] developed a procedure and correlations for estimating the Charpy impact energy and fracture toughness J-R curve of CASS based upon readily available material information. The correlations were based upon mechanical property results on CASS that were aged up to approximately 58000 at temperatures ranging from 290-350ºC (554 -662ºF). The extent of the thermal embrittlement was characterized by the room temperature Charpy impact energy. A correlation for the extent of thermal embrittlement following very long term aging was developed. This “saturation” or minimum impact energy was provided in terms of the chemical composition of the material tested

Screening Criteria

The recommended screening criteria discussed in Reference 7 are based on lower-bound values of the fracture toughness data in the literature. These toughness values are used in the flaw tolerance analysis of typical reactor coolant system geometries with representative service loading conditions to determine acceptable initial flaw sizes for inspections. The procedure is outlined in the following steps and shown graphically in Figure 2-1.

Low-molybdenum (e.g., SA 351 Grade CF-3 and CF-8) material that has been cast centrifugally is not subject to significant thermal aging embrittlement during exposure to service temperatures less than 320°C (610°F) for 525,000 hours (60 years). Low-molybdenum material that has been cast statically is not subject to potentially significant loss of fracture toughness after exposure to service temperatures less than 320°C (610°F) for 525,000 hours (60 years), provided that the delta ferrite content of the material can be shown by either calculation or measurement to be 20 %, or less. Management of potential loss of fracture toughness for low-molybdenum, statically-cast components is required, in terms of inservice examination and flaw evaluation program elements, if the delta ferrite content of the material cannot be shown to be 20 %, or less.

High-molybdenum (e.g., SA 351 Grade CF-3M and CF-8M) material that has been cast centrifugally is not subject to potentially significant loss of fracture toughness after exposures to temperatures less than 320°C (610°F) for 525,000 hours (60 years), provided that the delta ferrite content of the material can be shown by either calculation or measurement to be 20 %, or less. Management of potential reduction of fracture toughness for high-molybdenum, centrifugally-cast components is required, in terms of inservice examination and flaw evaluation program elements, if the delta ferrite content of the material cannot be shown to be 20 %, or less.

High-molybdenum (e.g., SA 351 Grade CF-3M and CF-8M) that has been cast statically is not subject to potentially significant loss of fracture toughness after exposures to temperatures less than 320°C (610°F) for 525,000 hours (60 years), provided that the delta ferrite content of the material can be shown by either calculation or measurement to be 14 %, or less. Management of potential reduction of fracture toughness for high-molybdenum, statically-cast components is required, in terms of inservice examination and flaw evaluation program elements, if the delta ferrite content cannot be shown to be 14 %, or less.

From the above, the most critical of all the components is the statically cast CF-3M and CF-8M CASS materials. Next is the centrifugally cast CF-3M and CF-8M materials which are expected to be used for most piping materials. Hence the focus of this study will be on the CF-8M CASS material

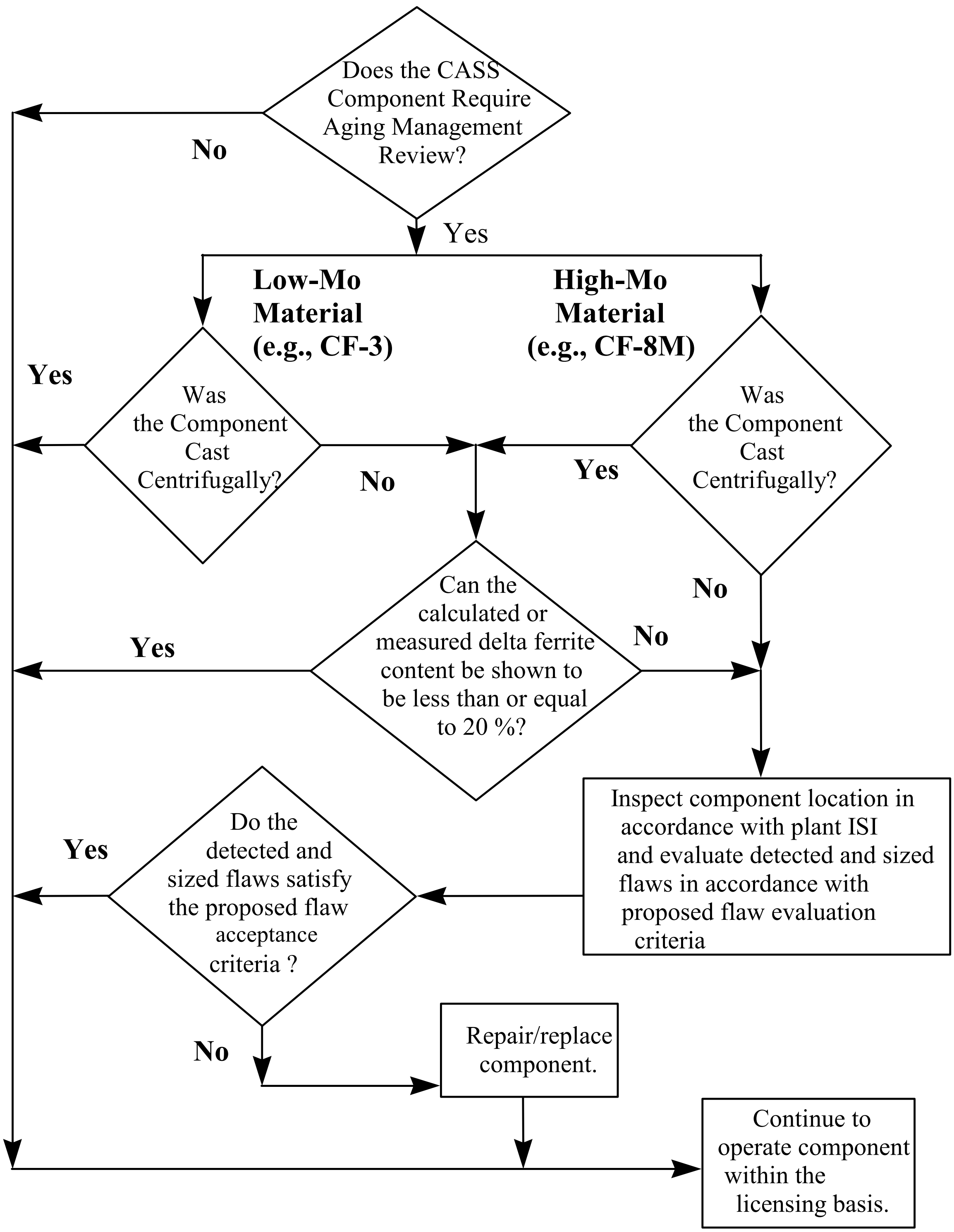

Figure 2-1
A Flaw Evaluation Method for CASS Piping Materials [7]

3

FLAW TOLERANCE APPROACH

Because of the challenges associated with the inspection of CASS components, especially piping welds, a proposed methodology to manage the structural integrity of CASS components is through the use of flaw tolerance evaluation. In this approach, a target flaw size for inspection is established based on fracture mechanics evaluations considering the material toughness, other material properties and the loading. The flowchart in Figure 3-1 provides a summary of the flaw tolerance evaluation to establish the target e inspection flaw size for CASS components. The methodology consists of determining the allowable flaw size (which includes ASME Section XI safety factors) for the component considering all possible degradation mechanisms (such as thermal aging), performing a flaw growth analysis to determine possible flaw growth during the inspection interval (or plant life) and using this information to establish a reasonable target flaw size that the inspection technology should be capable of detecting

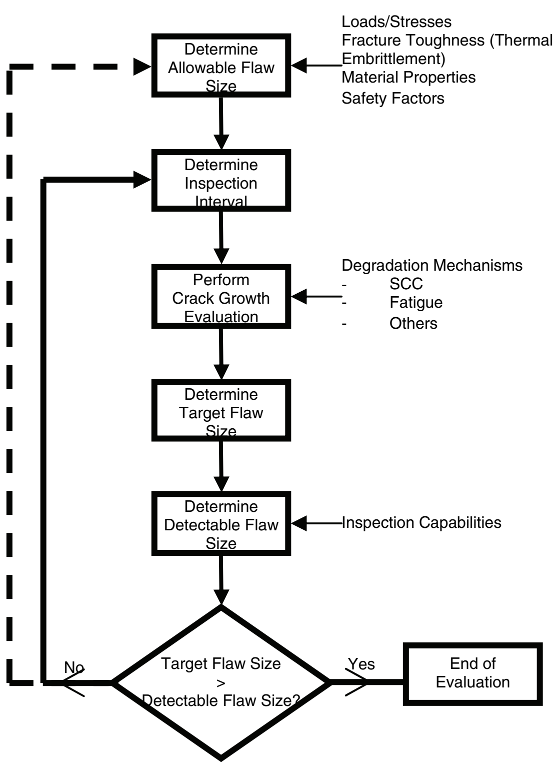

Figure 3-1
Flowchart for Flaw Tolerance Evaluation of CASS Components

A few studies have been performed in the literature to address the performance of aged CASS materials in the presence of a flaw that provide some insights into this study. Bamford and Linderman [8] performed a series of experiments with aged CF8M CASS pipe using four point bending test to compare the performance of the aged material as compared to the unaged condition. The test specimen used was a four inch schedule 80 pipe with thickness of 0.65 to 0.70 in. (16.5 mm to 17.8 mm). The ferrite levels in these components ranged from 6.7 FN to 12.7 FN. Circumferential crack starter notches were machined at the midspan of each of the test pipes and they were fatigued cracked before the load was applied. With the relatively low ferrite level in these specimens, it is not surprising that there was no significant difference in impact energy, J-R curves and maximum obtained load at failure between the aged and unaged specimens. Failure was by plastic instability as opposed to brittle failure. It was however noted in the paper that tests of more severely degraded material would add measurably to any conclusions.

Buchalet et al. [9] performed a flaw tolerance evaluation of CF8M CASS elbows in the aged and unaged condition using the R6 method. The load considered in this study included pressure, thermal expansion and LOCA loads. Finite length part through-wall flaws were considered both in the axial and circumferential directions. The critical flaw depths for the unaged conditions were 48 mm in the circumferential direction and 40 mm in the axial direction. For the aged condition, the critical flaw sizes reduced to 23mm and 26 mm respectively. The calculated crack growth was 6.0 mm in the circumferential direction and 6.7 mm in the axial direction.

Diaz et al. [10] also performed a flaw tolerance study on a large diameter CF8M CASS material using the deformation plasticity failure analysis diagram (DPFAD) as described in ASME Code Case N-494. The pipe diameter in this study was 349.25 mm and thickness of 56.77 mm. Circumferential cracks ranging from10% to 80% of wall thickness were addressed along with two lengths of circumferential flaws. Both normal operating and accident condition load combinations were considered in the study. For normal operating conditions, the allowable flaw depth was at least 50%. For accident conditions considering very high seismic loads, the allowable flaw depth is on the order of 15% of wall assuming a crack length of 180°. However when a crack length of 30° was considered, the allowable flaw depth increased to 50% of wall thickness. Furthermore, when the loading was reduce by half representing a relatively mild seismic stress, the allowable flaw depth even for the 180° length was at least 50% of wall thickness.

In this paper, a flaw tolerance approach is used to evaluate the acceptable flaw sizes (crack depth as a function of crack length) for typical cold leg piping of a PWR made from CASS material. Only circumferential cracks are considered in this initial preliminary study. Evaluation of several other configurations such as the surge line piping and axial flaws are pending. The pipe outside diameter is 32 inches (813 mm) with wall thickness of 2.25 inches (57 mm). The operating pressure is 2250 psi (15.5 MPa). A maximum design temperature of 650°F (343°C) was assumed in this study since thermal embrittlement is more pronounced at this temperature.

Fracture Toughness

The fracture toughness of CASS components is a key input into the flaw tolerance evaluation. Studies have shown that the fracture toughness of these components degrades with time as a result of thermal embrittlement (thermal aging) [4]. Unaged CASS components in general have adequate toughness comparable to wrought austenitic stainless steel as shown in Figure 3-2 [2] and as such, limit load (net section plastic collapse analysis can be used as the failure criterion for determining the allowable flaw size during the early life of the component. However, at reactor operating temperatures, the toughness of CASS components degrades such that elastic plastic fracture mechanics (EPFM) principle has to be used for determination of the allowable flaw size since the material has become semi-ductile at some time. With further operating time, the toughness may degrade to a point where the material has become brittle and as such, linear elastic fracture mechanics (LEFM) principles have to be used to determine the allowable flaw size. Figure 3-3 shows schematically how the fracture mechanics regime changes with time as a result of thermal aging. As illustrated in this figure, after significant exposure to thermal aging, the fracture toughness reaches a saturation value. This saturation value can be used as conservative fracture toughness in the flaw tolerance evaluation. The change in toughness with time has been the subject of research by various organizations, notably Argonne National Labs. The latest state-of-the art in determining the toughness of CASS components subject to thermal aging is documented in Reference 4

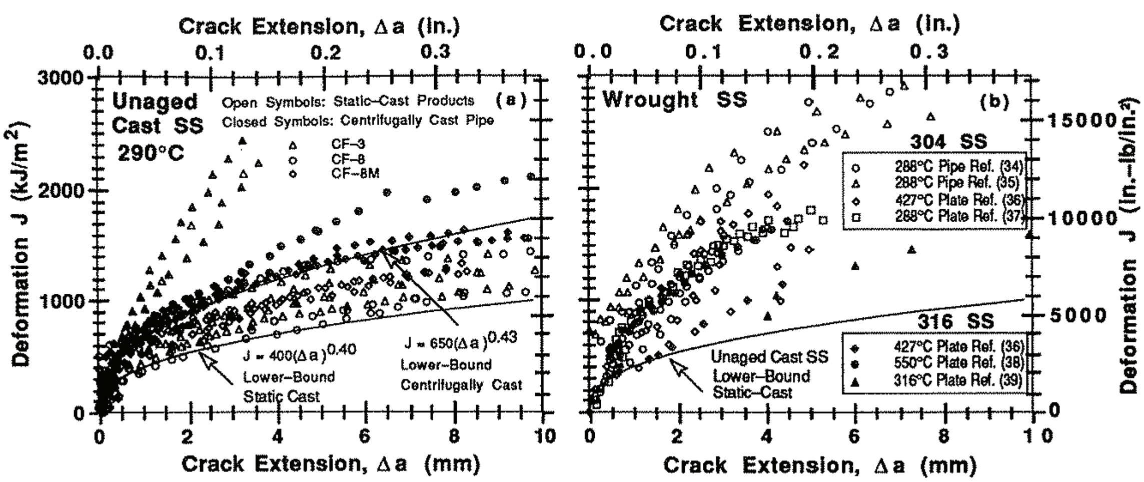

Figure 3-2
Comparison of Fracture Toughness of Unaged CASS Materials with Wrought Stainless Steel Materials [4

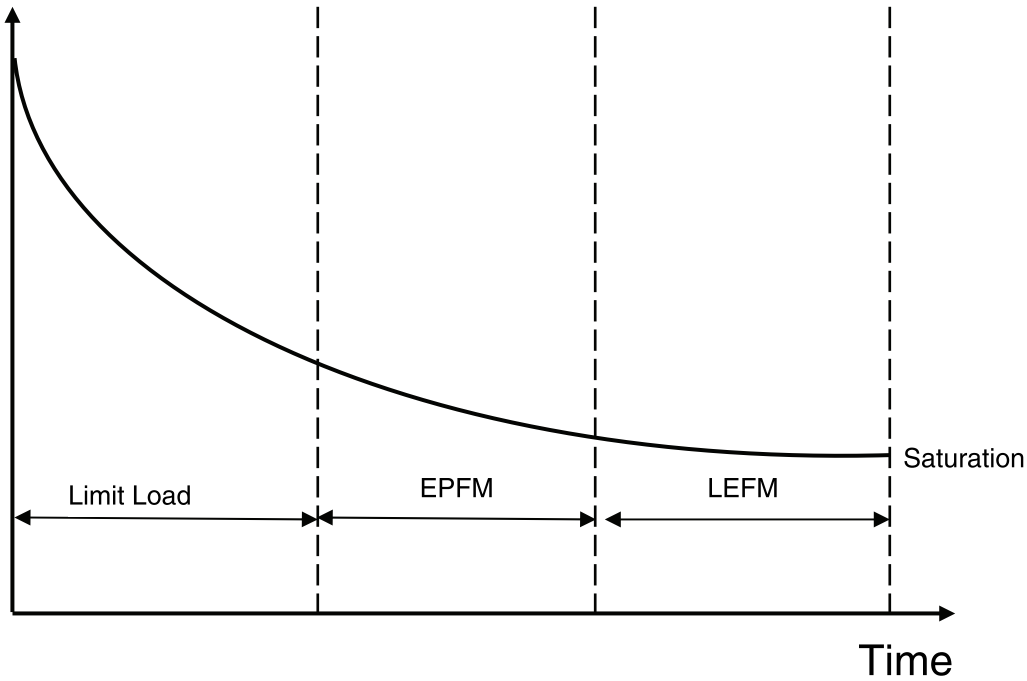

Figure 3-3
Change in Fracture Mechanics Regime for CASS Components Resulting From Thermal Aging

The fracture toughness is generally represented by the J-R resistance curve which is a material property which represents the material resistance to tearing. A procedure for determining the J-R curve parameters for CASS materials of known composition is provided in Reference 4. In this procedure, the chromium equivalent (Cr_{eq}) and nickel equivalent (Ni_{eq}) are determined from the chemical composition, based on Hull's equivalent factors [11]:

$$Cr_{eq} = (Cr) + 1.21\,(Mo) + 0.48\,(Si) - 4.99 \quad (3\text{-}1)$$

$$Ni_{eq} = (Ni) + 0.11\,(Mn) - 0.0086\,(Mn)^2 + 18.4\,(N) + 24.5\,(C) + 2.77 \quad (3\text{-}2)$$

where the chemical composition is in wt%. Per Reference 4, the value of N is assumed to be 0.04 if it is not available on the CMTR.

The ferrite content (δ_c) is then estimated from the relationship:

$$\delta_c = 100.3\,(Cr_{eq}/Ni_{eq})^2 - 170.72\,(Cr_{eq}/Ni_{eq}) + 74.22 \quad (3\text{-}3)$$

For CF8M CASS, the saturation (minimum) impact energy (Cv_{sat}) considering thermal embrittlement can be determined by two methods:

In the first method, the material parameter Φ is calculated from which Cv_{sat} is determined as follows:

$$\Phi = \delta_c (Ni + Si + Mn)^2 (C + 0.4N) / 5. \tag{3-4}$$

The saturation value of RT impact energy, Cv_{sat}, for steels with < 10% Ni is given by

$$Log_{10}\, Cv_{sat} = 1.10 + 2.12 exp(-0.041 \Phi). \tag{3-5}$$

And for steels with >10% Ni by

$$Log_{10}\, Cv_{sat} = 1.10 + 2.64 exp(-0.064 \Phi). \tag{3-6}$$

In the second method, Cv_{sat} is estimated directly from the chemical compositions of the steel and is given by:

$$Log_{10}\, Cv_{sat} = 7.28 - 0.011 (\delta_c) - 0.185 (Cr) - 0.369 (Mo) - 0.451 (Si) \tag{3-7}$$

$$- 0.007 (Ni) - 4.71 (C + 0.4N)$$

The saturation impact energy is determined using both methods given in Equations 3-5, 3-6 and 3-7 and the lower value is used for estimating the fracture toughness.

The material resistance J-R curve can be estimated from Cv_{sat} using a power law relationship:

$$J_d = C [Cv_{sat}]^m [\Delta a]^n \tag{3-8}$$

where: J_d is the deformation J-Integral (kJ/m^2) per ASTM Specification E813-85

Δa is the crack extension (mm)

C is a constant

m, n are power law exponents

The saturation fracture toughness J-R curve at room temperature for centrifugally-cast CF8M stainless steel is given by [4]:

$$J_d = 20[Cv_{sat}]^{0.67} [\Delta a]^n \tag{3-9}$$

In English units, the J-R curve (units of J in in-kips/in^2 and Δa in inches) is given by:

$$J_d = 114[25.4]^n [Cv_{sat}]^{0.67} [\Delta a]^n \tag{3-10}$$

where Cv_{sat} is in Joules/cm^2 and the value of n at room temperature is given by:

$$n = 0.25 + 0.077 \log_{10} Cv_{sat} \tag{3-11}$$

Corresponding equations for the J-R curve at temperatures between 290ºC and 350ºC (550ºF and 662ºF) are given by:

$$J_d = 57[Cv_{sat}]^{0.41}\,[\Delta a]^n \text{ (SI units)} \tag{3-12}$$

$$J_d = 325[25.4]^n[Cv_{sat}]^{0.41}[\Delta a]^n \text{ (English units)} \tag{3-13}$$

$$n = 0.23 + 0.057\log_{10} Cv_{sat} \tag{3-14}$$

Equation 3-13 for the J-R curve can be expressed in simple terms as:

$$J_d = C\,[\Delta a]^n \tag{3-15}$$

The above correlations (Equations 3-1 through 3-15) account for degradation of toughness due to thermal aging, but do not explicitly consider the initial fracture properties of the original unaged material. Fracture toughness data in Reference 4 indicate that the J-R curve for some heats of unaged cast stainless steel may be lower than those for wrought stainless steel. To take into account the possibility of a relatively low initial unaged toughness, the methodology outlined in Reference 4 requires that the saturation J-R curves be compared to the lower bound J-R curve for the unaged cast stainless steel. The lower of the two curves is then used. For statically cast stainless steel, the lower bound unaged J-R curve is given by:

$$J_d = 400\,[\Delta a]^{0.40} \text{ (SI units)} \tag{3-16}$$

$$J_d = 8330\,[\Delta a]^{0.40} \text{ (English units)} \tag{3-17}$$

The above equations were used to determine the values of the parameters C and n for a set of Grade CF8M CASS material spool pieces for one piping system for which the chemical compositions were readily available. The variation of C and n as a function of delta ferrite content for this material set is shown in Table 3-1. Also shown in Table 3-1 is the elastic-plastic fracture toughness, J_{1C}. As can be seen, the parameter C is a strong function the delta ferrite content while the parameter n is unaffected. The resulting aged material J-R curves used in this study are shown in Figure 3-4.

Table 3-1
J-R Curve Parameters vs. Delta Ferrite Number (DFN)

DFN	J_{1C}		C		n
	in-lb/in^2	kJ/m^2	in-lb/in^2	kJ/m^2	
15	1000	175	5750	325	0.35
20	915	160	5200	294	0.35
25	800	140	4500	254	0.35
30	650	114	3610	204	0.35

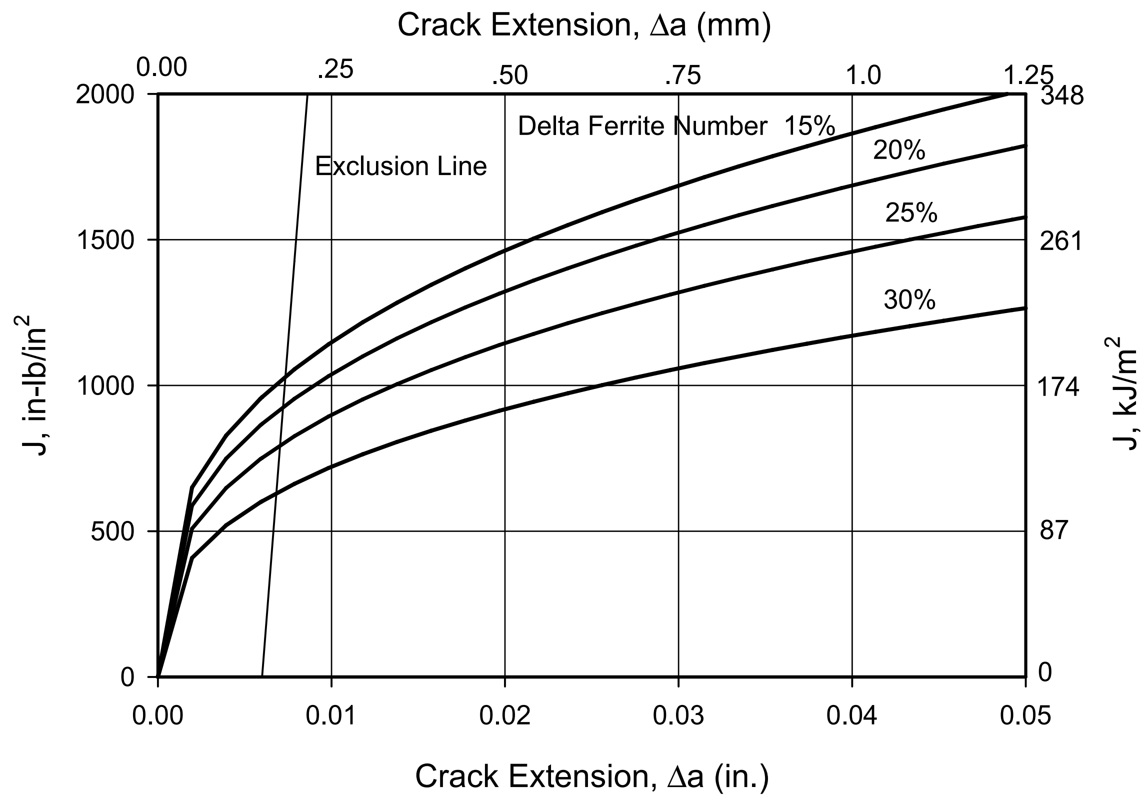

Figure 3-4
Aged J-R Material Resistance Curves for Grade CF8M CASS at Various DFN Levels

Stress-Strain Properties

In addition to the fracture toughness, other material properties that are of importance in flaw tolerance evaluation are the yield and ultimate strengths of the material as well as the Ramberg-Osgood parameters describing the stress-strain curve of the material. Studies performed in Reference 12 indicate that in general, thermal aging leads to an increase in both yield and ultimate strength and a slight decrease in ductility. The ratios of aged versus unaged tensile properties are shown in Figure 3-5. In some case however, there is a slight decrease in tensile properties with aging. In general, there is a very mild increase in the ultimate strength as a function of delta ferrite for the unaged material for the representative spool piece considered in this evaluation. The yield strength is virtually unaffected by the delta ferrite content in the unaged condition. In this study, the beneficial increase in tensile properties will not be taken into account and the unaged properties will be used.

The Ramberg-Osgood stress-strain parameters are represented by the expression:

$$\frac{\varepsilon}{\varepsilon_0} = \frac{\sigma}{\sigma_0} + \alpha \left[\frac{\sigma}{\sigma_0}\right]^n \qquad (3\text{-}18)$$

where σ and ε are true stress and true strain, respectively, and ε_0, σ_0, α and n are model parameters that must be determined for the material of interest. The parameters σ_0 and ε_0 are reference stress and strain, respectively. Usually, σ_0 is taken as the yield stress, σ_y, and ε_0 is taken to be the pseudo-elastic yield strain (σ_y/E). If the stress-strain curve of the material is available, these parameters can be determined by curve fitting.

The Ramberg-Osgood parameters used in this study are shown in Table 3-2.

Table 3-2
Stress-Strain Curve Parameters

E	σ_y	σ_u	α	n
25.6×10^3 (ksi) 176×10^3 (MPa)	29 (ksi) 200 (MPa)	85.4 (ksi) 589 (MPa)	1.282	6.408

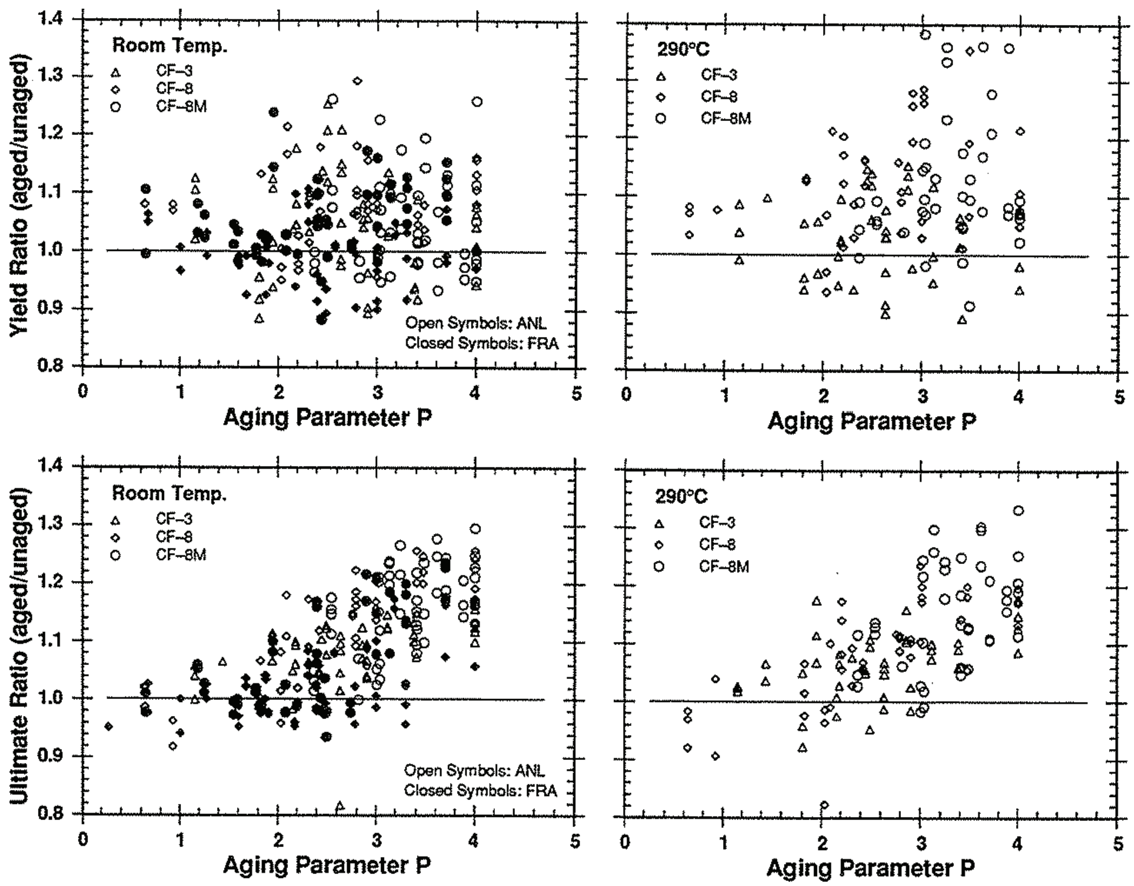

Figure 3-5
Ratio of Yield and Ultimate Stress of Aged and Unaged Cast Stainless Steel as a Function of Aging Parameter P [12]

Loads and Stresses

The stresses required to calculate the allowable flaw size are typically available in the Stress Report for the component. Loads/stresses are required for all operating conditions defined in ASME Code, Section III (Levels A, B, C and D). The stresses may be due to a combination of primary loads as well as secondary loads. For piping components, the primary bending stress in ASME Code, Section XI correspond to the unconcentrated primary stresses defined in Equation (9) of ASME Code, Section III, Section NB-3650. The secondary (expansion) stress is the unconcentrated stress intensity value for loads defined in Equation (10) of ASME Code, NB-3650. A limited study performed on a few Stress Reports indicate the load combination for the bending stress, normal operating and upset conditions (dead weight, thermal and OBE seismic) which typically bound the flaw evaluation is between 5 ksi (34.5 MPa) and 10 ksi (68.9 MPa) for CASS piping components. In addition to these loads, transient thermal stresses and residual stresses were considered in Reference 10. However in this study, these additional stresses will not be considered since they are not required in determining allowable flaw size by ASME

Section XI when considering EPFM or limit load. Thus, the two stress limits are consistent with the normal operating cases in Reference 10. These two stresses will be used in the study herein. Nevertheless, the methodology provided can be applied on a component specific basis once the stresses and other material parameters are established to demonstrate the range of flaw depths, lengths and corresponding margins on loads for the CASS cold leg piping.

Allowable Flaw Size Determination

In the previous studies [9, 10], the DPFAD approach was used to establish the allowable flaw size. Furthermore the DPFAD analysis in Reference 10 indicated that the analysis for the critical or allowable flaw size fall into the EPFM regime. In this study, the allowable flaw sizes are determined by considering both EPFM and limit load. The limit load solution can be used in cases where the material is not severely embrittled.

Elastic Plastic Fracture Mechanics Evaluation

In this study, EPFM analyses involving the J-integral/tearing modulus (J/T) analyses are used to determine the critical through-wall flaw sizes. Simple handbook solution has been developed for calculating J for cracks in various cylindrical configurations [13, 14]. For a cylinder under tension and bending loads the J-integral is given by [13]:

Tension:

$$J = f_t \; P^2 / \left(4\pi R^2 tE'\right) + \alpha\sigma_o\varepsilon_o t \, H_1 \left(\sigma_t / \sigma_o\right)^{n+1} \qquad (3\text{-}19)$$

Bending:

$$J = f_b \; M^2 / \left(4\pi R^4 tE'\right) + \alpha\sigma_o\varepsilon_o t \; H_1 \left(\sigma_b / \sigma_o\right)^{n+1} \qquad (3\text{-}20)$$

The Tearing Modulus (T) is defined by the expression:

$$T = \frac{dJ}{da}\frac{E}{{\sigma_f}^2} \qquad (3\text{-}21)$$

Hence, in calculating T, J from the above expressions is determined as a function of crack size (a) and the slope of the J versus crack size (a) curve is calculated in order to determine T. (The flow stress, σ_f, is taken as the mean of the yield and ultimate tensile strengths.) The material resistance J-R curve can also be transformed into J-T space in the same manner. The intersection of the applied and the material J-T curves is the point at which instability occurs and the crack size associated with this instability point is the critical crack size.

The piping stresses consist of both tension and bending stresses. The tension stress is due to internal pressure and axial forces while the bending stress is caused by deadweight, thermal and seismic moments. Because a fracture mechanics model for combined tension and bending loading is not readily available, the critical flaw length under such loading condition was determined using the tension and bending models separately. For the first case, the stress combination is assumed to be all due to tension and the critical flaw length is determined using the tension model. For the second case, the stress combination is assumed to be all due to bending and the critical flaw length is determined as such. The half critical flaw sizes (lengths) obtained with the tension model (a_t) and the bending model (a_b) are combined to determine the actual half critical flaw size (a_c) due to a combined tension and bending stress using linear interpolation, as described by the following equation:

$$a_c = a_t \frac{\sigma_t}{\sigma_b + \sigma_t} + a_b \frac{\sigma_b}{\sigma_b + \sigma_t} \tag{3-22}$$

where σ_t and σ_b are the piping tensile and bending stresses respectively. In determining the critical flaw sizes, the following assumptions were made

For this preliminary study, two different safety factors were considered in performing this analysis. In the first case, a safety factor of unity was considered which provides the critical flaw size. Secondly, the ASME Section XI safety factor of 2.77 (for Service Level A/B) was applied to determine the allowable flaw size. The upper and lower bound J-R curves shown in Figure 3-4 were used to determine the allowable flaw size. The results of the evaluation are shown in Figures 3-6 and 3-7 for stresses of 5 ksi (34.5 MPa) and 10 ksi (68.9 MPa), respectively. It can be seen that with a safety factor of unity, the target flaw depths are relatively high. However, when the Code safety margin is applied the target flaw size reduces.

Limit Load Analysis

Limit load analysis can be used only if it is demonstrated that the material has adequate toughness as in the unaged condition. The net section collapse methodology described in Reference 15 and implemented in ASME Code Section XI, Appendix C [16] is used in this evaluation. The technical approach consists of determining the allowable flaw size (circumferential extent and through-wall depth) in the pipe that will cause the flawed pipe section to collapse. Based on equilibrium of longitudinal forces and moments about the pipe axis, the relation between the applied loads and flaw size at incipient plastic collapse is given by:

$$P'_b = \frac{2\,\sigma_f}{\pi}\left(2\sin\beta - \frac{a}{t}\sin\alpha\right) \tag{3-23}$$

where the angle, , defining the location of the neutral axis is:

$$\beta = \frac{1}{2}\left(\pi - \frac{a}{t}\alpha - \pi\frac{P_m}{\sigma_f}\right) \tag{3-24}$$

α	=	half flaw angle
t	=	pipe thickness
a	=	flaw depth

P_m = primary membrane stress

P'_b = bending stresses corresponding to plastic collapse

σ_f = flow stress at net section plastic collapse ($3S_m$).

For longer flaws penetrating the compressive bending region where $(\alpha + \beta) > \pi$, the relation between the applied loads and the flaw depth at incipient plastic collapse is given by:

$$P'_b = \frac{2\,\sigma_f}{\pi}\left(2 - \frac{a}{t}\right)\sin\beta \tag{3-25}$$

where:

$$\beta = \frac{\pi}{2 - \frac{a}{t}}\left(1 - \frac{a}{t} - \frac{P_m}{\sigma_f}\right) \tag{3-26}$$

An iterative process is used to calculate the allowable a/t for a given flaw length using Equations 3-23 through 3-26. The value of σ_f is taken as $3S_m$ as recommended in Reference 15. The results of the evaluation are presented in Figures 3-8 and 3-9 for the 5 ksi (34.5 MPa) and 10 ksi (68.9 MPa) case respectively. Two values of S_m were used for the evaluation. The first is that determined by using the minimum ASME Section III Code value of 16.7 ksi (115 MPa) for S_m. The second approach is to use the S_m value of 26.1 ksi (180 MPa) corresponding to the actual material properties. Using the actual material properties data resulted in much higher allowable flaws depths as shown in Figure 3-8 and 3-9.

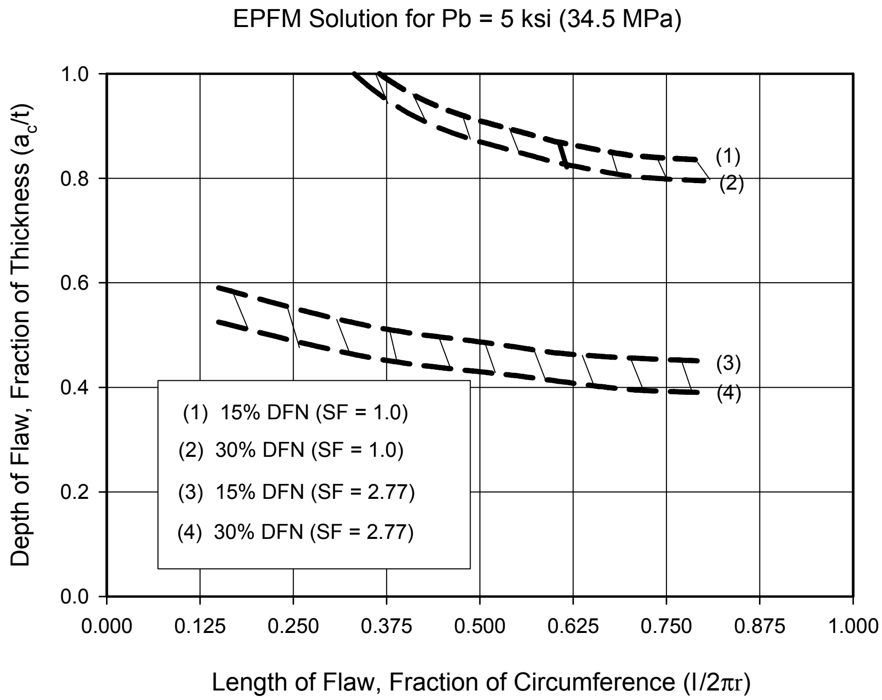

Figure 3-6
Critical and Allowable Flaw Sizes (EPFM – 5ksi Bending Stress)

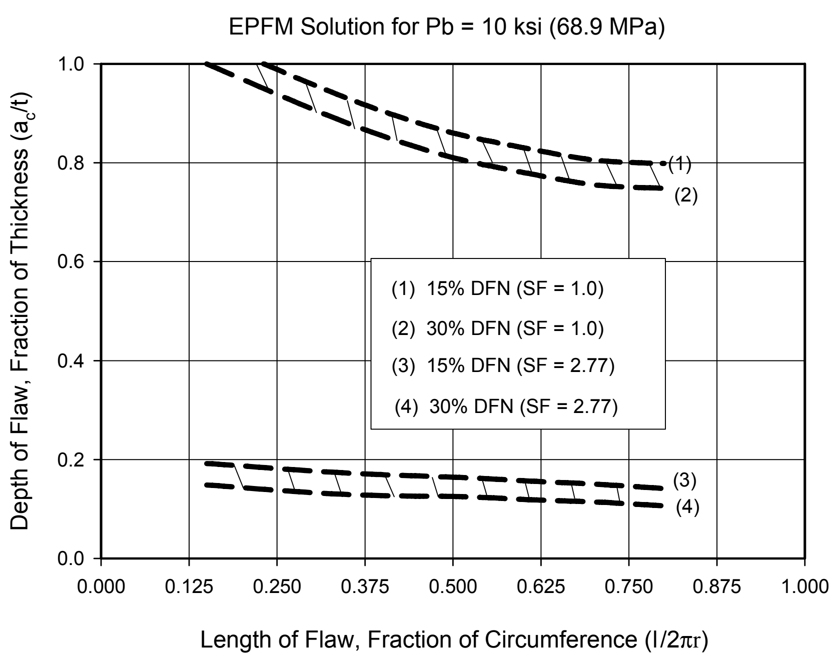

Figure 3-7
Critical and Allowable Flaw Sizes (EPFM – 10 ksi Bending Stress)

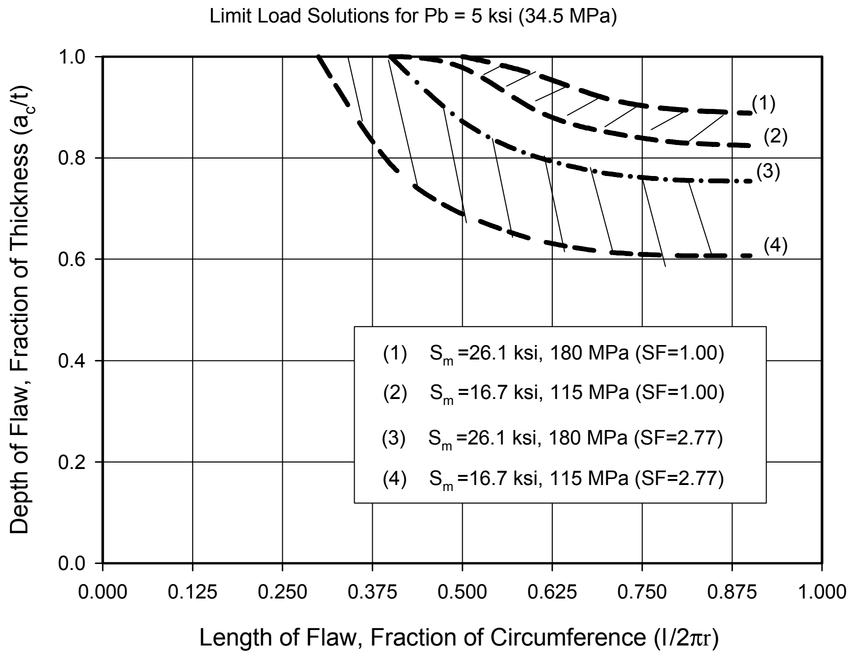

Figure 3-8
Critical and Allowable Flaw Sizes (Limit Load – 5 ksi Bending Stress)

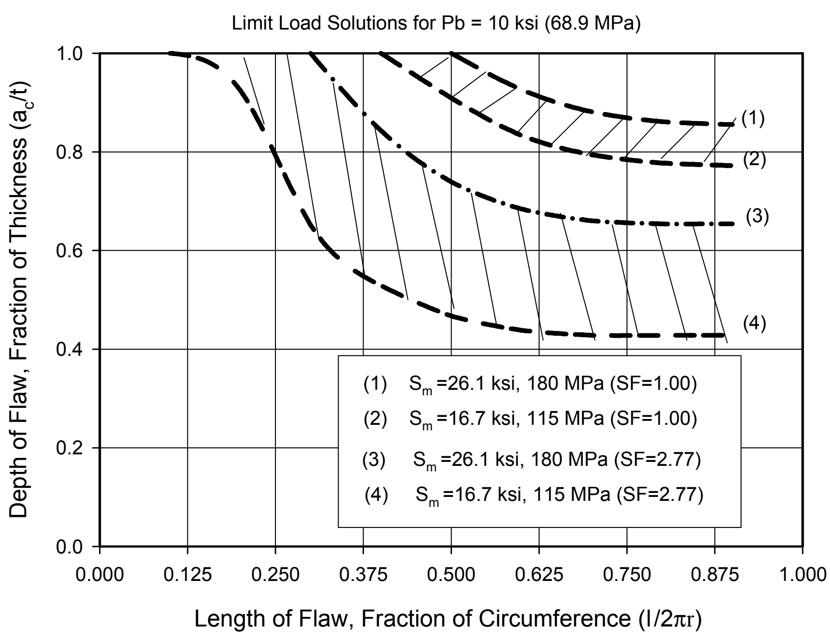

Figure 3-9
Critical and Allowable Flaw Sizes (Limit Load – 10 ksi Bending Stress)

Crack Growth Considerations

To determine the target flaw size for inspection, the expected crack growth at the time of next inspection has to be estimated and subtracted from the allowable flaw size. The transients for the cold leg consist of the normal transients defined in the original plant design. In general, the transients are dominated by the normal heat-up and cool-down transients and all other intermediate transients contribute little to fatigue crack growth. For other piping systems such the surge line, stratification related transients need to be also addressed as well in the evaluation. Weld residual stresses, even though they are not cyclic, are also included in the crack growth evaluation since they affect the R ratio. The crack growth law from ASME Section XI, Appendix C for stainless steel in air environment is used with an additional factor of two applied to account for the PWR environment [15]. For the cold leg piping, the crack growth for a 10 year period is relatively small (on the order of 0.1 inch or 2.5 mm). This is consistent with the findings in Reference 9. Hence, in determining the acceptable flaw sizes for inspections, these crack growth results should be subtracted from the allowable flaw sizes presented in Figures 3-6 through 3-8.

4 SUMMARY, CONCLUSIONS AND RECOMMENDATIONS

The flaw evaluation standards for austenitic piping in ASME Section XI, IWB-3514-2, and the flaw evaluation procedures given in IWB-3640, define the limiting acceptable flaw sizes for flaws that are detected inservice. Austenitic piping materials including CASS materials are known to have significantly high toughness properties even in the aged condition, and evaluations of flaws requires the use of EPFM or limit load analyses to accurately characterize the critical and allowable flaw sizes to maintain these Code margins. The EPFM and limit load results shown in Section 3.4 for the typical cold leg piping in a PWR show that the critical flaw sizes for normal operating stresses are on the order of 80% through wall and 75% of the pipe circumference. The allowable through-wall flaw size with a safety factor of 2.77 is about 40 – 50% of the pipe thickness for the operating stresses. The difference between these values demonstrates the safety margin that is inherent in the Code. For those materials and components that experience active crack growth (e.g., PWSCC), these margins are normally maintained by performing regular inspections to demonstrate that flaws of this size are not present.

The CASS piping materials do not experience a known active crack growth mechanism; however, there is a reduction in the toughness due to thermal aging of the material. It is possible to manage the change in toughness of these materials through a fracture mechanics analyses to demonstrate the structural integrity of the piping throughout the intended service life assuming flaws do not exceed the critical flaw size of some length and depth (to be determined). The analyses presented in this report provide an indication of the critical and allowable flaw sizes to assist in the determination of acceptable flaw sizes. Since crack growth is not a major concern, as discussed in Section 3.5, the flaws of interest are primarily fabrication flaws that were not detected during preservice inspections. Since crack growth is minimal, the acceptable flaw size (i.e., maximum allowable flaw size minus the provision for crack growth) is very close to that calculated allowable flaw size.

This preliminary report has presented a flaw tolerance approach based on fracture mechanics considerations that can be used for management of CASS piping inspection. The following are conclusions from the study:

- Target flaw sizes for the cold leg piping considered are very much dependent on the loads and safety factor used in the analysis. For the case where the safety margin is unity (i.e., for critical flaw size), relatively large flaw sizes are obtained even with relatively high loads. When the ASME Code safety margin is applied, the target flaw sizes are smaller.
- Crack growth for non surge line locations is very minimal and therefore, the acceptable flaw size (allowable flaw size minus provision for crack growth) is very close to the allowable flaw size.
- For the management of CASS components, a few conservatisms inherent in the flaw evaluation procedure, if addressed, can improve the results appreciably. First of all, the full ASME Section XI safety factor reduced the targetflaw size considerably. If this safety factor was reduced, the allowable flaw size would increase. It was also shown that in the case of

limit load analysis, if the actual material properties rather than the Code values are use, the targetflaw sizes would increase. These considerations should be taken into account in developing a comprehensive management program for CASS piping in nuclear power plants.

The study contained in this report used the cold leg piping as an example to develop the flaw tolerance methodology for CASS piping. Future potential studies to build on the initial study in this report include the following:

- In this study, both elastic-plastic fracture mechanics techniques and limit load analysis was used to determine the critical and allowable flaw sizes. It was shown that significant benefit can be obtained in limit load analysis is used to determine these parameters. Criteria similar to that in ASME Section XI, Appendix C for ferritic steels should be considered for CASS materials in order to determine the analysis regime to be used for the evaluation.

- Only a limited number of Stress Reports were reviewed to determine the bounding stresses that were used for the evaluation. An expanded search should be made to establish loads for the full range of affected CASS piping components in the industry.

- Only one component (cold leg piping) was used in this initial study. Flaw acceptance diagrams should also be developed for other CASS components.

- Although circumferential flaws are believed to be limiting, the study should be expanded to axial flaws for all critical CASS components.

- Interaction with the industry (e.g. ASME Code and Owners Groups) to define appropriate parameters (such as loadings and safety factors) that can be used to effectively manage the structural integrity of CASS piping considering the NDE capabilities and other factors such as the resistance of CASS components to various degradation mechanisms documented in the industry.

- In the longer term, probabilistic approaches should be considered due to the variability of many of the important parameters.

5
REFERENCES

1. Cast Stainless Steels, Knowledge Article from www.Key-to-Steel.com
2. M. T. Anderson, S. L. Crawford, S. E. Cambridge, K. M. Denslow, A. A. Diaz, S. R. Doctor, "Assessment of Crack Detection in Heavy-Walled Cast Austenitic Cast Stainless Steel Piping Welds Using Advanced Low-Frequency Ultrasonic Methods," NUREG/CR-6933, PNNL-16292, Pacific Northwest National laboratory, March 2007.
3. A. Diaz, R. A. Mathews, J. Hixon, S. R. Doctor, "Assessment of Eddy Current Testing for the Detection of Cracks in Cast Stainless Steel Reactor Piping Components," NUREG/CR-6929, PNNL-16253, Pacific Northwest National Laboratory, February 2007.
4. K. Chopra, "Estimation of Fracture Toughness of Cast Stainless Steels During Thermal Aging in LWR Systems", NUREG/CR-4513, ANL-93/22, Rev. 1, Argonne National Laboratory, August 1994.
5. "Assessment and Management of Ageing of Major Nuclear Power plant Components Important To Safety-Primary Piping in PWRs", IAEA-TECDOC-1361, International Atomic Energy Agency, July 2003.
6. J. Giannuzzi, "LWR Experience With Centrifugally Cast Stainless Steel Pipe", EPRI NP-4996-LD, December 1986.
7. R. E. Nickell, and M. A. Rinckel, "Evaluation of Thermal Aging Embrittlement for Cast Austenitic Stainless Steel Components", EPRI Final Report 1000976, January 2001.
8. W. H. Bamford and E. I. Landerman, "Thermal Aging of Cast Stainless Steel, and Its Impact on Piping Integrity", Journal of Engineering Materials and Technology, Volume 107, January 1985.
9. Buchalet, Y Meyzaud, Ph. Taupin, "Effect of Ling Term Aging On The Critical Defect Sizes In Primary Piping Cast Stainless Steel Elbows", Proceedings of the Second International Symposium on Environmental Degradation of Materials In Nuclear Power Systems-Water Reactors, Monterey, California, September 9-12, 1985.
10. A. Diaz, S. R. Doctor, B. P. Hildebrand, F. A. Simonen, G. L. Schuster, E. S. Andersen, G. P. McDonald, R. D. Hasse, "Evaluation of Ultrasonic Inspection Techniques for Coarse-Grained Materials", NUREG/CR-6594, PNNL-11171, Pacific Northwest National Laboratory, October 1998.
11. L. S. Aubrey, P. F. Wieser, W. J. Pollard, and E. A. Schoefer, "Ferrite Measurement and Control in Cast Duplex Stainless Steel," in Stainless Steel Castings, V. G. Behal and A. S. Melilli, editors, ASTM STP 756, pp. 126-164 (1982).
12. W. F. Michaud, P. T. Toben, W. K. Soppert, O. K. Chopra, "Tensile-Property Characterization of Thermally Aged Cast Stainless Steels," NUREG/CR-6142, February 1994.
13. Zahoor, "Ductile Fracture Handbook," Vol. 3, EPRI Report NP-6301-D, June 1989.
14. V. Kumar and M. D. German, "Elastic-Plastic Fracture Analysis of Through-Wall and Surface Flaws in Cylinders," EPRI Report No. NP-5596, January 1988.

15. Section XI Task group for Piping Flaw Evaluation, ASME Code, "Evaluation of Flaws in Austenitic Steel Piping," Journal of Pressure Vessel Technology, Vol. 108, August 1986, PP 352-366.
16. ASME Boiler and Pressure Vessel Code, Section XI, 1998 Edition.

Export Control Restrictions

Access to and use of EPRI Intellectual Property is granted with the specific understanding and requirement that responsibility for ensuring full compliance with all applicable U.S. and foreign export laws and regulations is being undertaken by you and your company. This includes an obligation to ensure that any individual receiving access hereunder who is not a U.S. citizen or permanent U.S. resident is permitted access under applicable U.S. and foreign export laws and regulations. In the event you are uncertain whether you or your company may lawfully obtain access to this EPRI Intellectual Property, you acknowledge that it is your obligation to consult with your company's legal counsel to determine whether this access is lawful. Although EPRI may make available on a case-by-case basis an informal assessment of the applicable U.S. export classification for specific EPRI Intellectual Property, you and your company acknowledge that this assessment is solely for informational purposes and not for reliance purposes. You and your company acknowledge that it is still the obligation of you and your company to make your own assessment of the applicable U.S. export classification and ensure compliance accordingly. You and your company understand and acknowledge your obligations to make a prompt report to EPRI and the appropriate authorities regarding any access to or use of EPRI Intellectual Property hereunder that may be in violation of applicable U.S. or foreign export laws or regulations.

The Electric Power Research Institute (EPRI)

The Electric Power Research Institute (EPRI), with major locations in Palo Alto, California; Charlotte, North Carolina; and Knoxville, Tennessee, was established in 1973 as an independent, nonprofit center for public interest energy and environmental research. EPRI brings together members, participants, the Institute's scientists and engineers, and other leading experts to work collaboratively on solutions to the challenges of electric power. These solutions span nearly every area of electricity generation, delivery, and use, including health, safety, and environment. EPRI's members represent over 90% of the electricity generated in the United States. International participation represents nearly 15% of EPRI's total research, development, and demonstration program.

Together…Shaping the Future of Electricity

Printed on recycled paper in the United States of America

1016236

Electric Power Research Institute
3420 Hillview Avenue, Palo Alto, California 94304-1338 • PO Box 10412, Palo Alto, California 94303-0813 • USA
800.313.3774 • 650.855.2121 • askepri@epri.com • www.epri.com